Optics Communications 381 (2016) 140–145

Contents lists available at ScienceDirect

Optics Communications

journal homepage: www.elsevier.com/locate/optcom

# Quantum dots lasers dynamics under the influence of double cavity external feedback

S.S. Rusu, T. Oloinic, V.Z. Tronciu *

*Department of Physics, Technical University of Moldova, bd. Stefan cel Mare 168, Chisinau MD-2004, Republic of Moldova*

ARTICLE INFO

*Article history:*
Received 24 March 2016
Received in revised form
9 June 2016
Accepted 29 June 2016
Available online 13 July 2016

*Keywords:*
Quantum dots semiconductor lasers
Optical feedback
Bifurcations

ABSTRACT

This paper reports results on investigations of the dynamical behavior of a semiconductor laser with quantum dots active medium under the influence of a feedback from double external cavity. This configuration is treated in the framework of Lang-Kobayashi equations. The locus of external cavity modes is found to be elliptic, as in case of conventional optical feedback, but also represents different shapes, even with possible satellite bubbles. A bifurcation analysis is carried out revealing the points of saddle-node and Hopf bifurcations. Finally, the nature of bifurcations and the stability of steady state solutions are analyzed in dependence on different parameters.



## 1. Introduction

During recent years, the phenomena of control and stabilization, as well as the destabilization and chaos of laser emission by external cavities have received considerable attention due to its fundamental and applied interests. The main aim of technological progress is the production of structures with stable properties and the possibility of their application in different areas.

Stabilization of laser emission by external cavities has a long history [1–5] and is still of continuous interest [6–10]. Another well-known method of control is due to Pyragas [11] applied successfully to different systems [12–14]. The control of a laser subject to conventional optical feedback was studied in [15] where it was shown that by using a second branch and properly adjusting the feedback delays and strengths complex dynamical regimes can be stabilized. These control techniques found certain applications in information transmission systems.

On the other hand, different dynamical behaviors have been obtained for lasers under the influence of feedback from external cavities, including periodic and quasi-periodic pulsations, low frequency fluctuations, coherent collapse, optical turbulence, chaos (for more details, see [16]). The chaotic waveform is suitable for chaos-based communications. Recently, chaotic communications have become an option to improve privacy and security in date transmission, especially after the recent field demonstration of the metropolitan fiber networks of Athens [17]. In optical chaos-based communications, the chaotic waveform is generated by using semiconductor lasers with either all-optical or electro-optical feedback loops [18,19]. In particular, synchronized chaotic waveforms have found applications in chaos based communication systems.

Due to the continuing technological progress, lasers with active medium quantum dots have reach stable operation. Lasers with active medium quantum dots are compact and good candidacy for both applications: stabilization of laser emission and for chaos-based communications. Arakawa [20] predicted that semiconductor lasers with active medium quantum dots have small temperature dependence performance than the existing semiconductor lasers, and that they will not degrade at the high temperature. Other advantages of lasers with quantum dots active medium include the reduction of the threshold current and increase of the amplification coefficient [21]. In recent years, their dynamics has become the object of study and theoretical researches are necessary for the development and extension of the theory of nonlinear dynamics in semiconductor lasers with quantum dots active medium. Here we consider a configuration which includes feedback from an integrated double cavity. The paper is organized as follows. The device structure and mathematical model are described in Section 2. Section 3 is devoted to the analysis of stationary states. A detailed study of the dynamical properties of quantum dots lasers under the influence of double cavity feedback are discussed in Section 4. Finally, conclusions are drawn in Section 5.

## 2. Model and equations

In this paper, we focus on the investigation of the dynamical behavior of semiconductor lasers with quantum dots active

* Corresponding author.
*E-mail address:* tronciu@mail.utm.md (V.Z. Tronciu).

http://dx.doi.org/10.1016/j.optcom.2016.06.082
0030-4018/

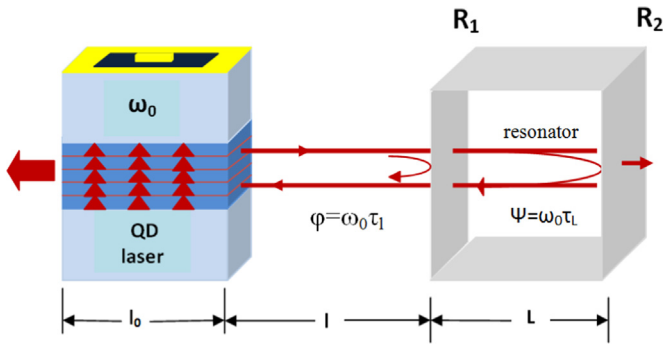


**Fig. 1.** Laser setup. $l_0$ is the length of the laser, $l$ is the distance between back facet of laser and the first mirror of resonator. $L$ is the distance between first and second mirrors, $\omega_0$ is free running frequency of laser, $\varphi$ is the feedback phase of the air gap, and $\psi$ is the phase within the resonator. $\tau_l$ and $\tau_L$ are external cavities round trip times.

medium shown in Fig. 1. The setup consists of laser operating under the influence of an external optical feedback from double cavity. The first mirror is located at distance $l$ from the laser front facet. The distance between first and second mirrors is $L$. The phase $\varphi$ in the air gap can be changed by a piezo-element. The optical feedback phase $\psi$ in the second cavity can be controlled by injecting current into the passive section. We assume that the current injected into passive section is small enough to affect only the refractive index, so that the optical length of the resonator is changed in the sub-wavelength range. On the other hand, the feedback phase $\varphi$ can be tuned, by the change in the delay time between the two mirrors.

For modeling of the dynamics of quantum dots laser under the influence of double optical feedback we use the following equations [22,23] for dimension less quantities

$$\frac{dE}{d\tau} = \frac{1}{2}(1+i\alpha)\Big[-\gamma_{np} + g(2\rho-1)\Big]E + \Gamma_1 e^{-i\varphi}E(\tau-\tau_l) + \Gamma_2 e^{-i(\varphi+\psi)}E(\tau-(\tau_l+\tau_L)), \quad (1)$$

$$\frac{d\rho}{d\tau} = -\gamma_{ns}\rho - (2\rho-1)|E|^2 + (CN^2+BN)(1-\rho), \quad (2)$$

$$\frac{dN}{d\tau} = J - N - 2\Big[(CN^2+BN)(1-\rho)\Big], \quad (3)$$

where $E$ is the complex amplitude of the electric field, $N$ is the carrier density in the quantum well, and $\rho$ is the occupation probability in the quantum dot. $\tau_l$=0.05, $\tau_L$=0.2 are external cavity round trip times which correspond to $l$=7.5 mm, and $L$=1 cm, respectively. $g$=1200 is the differential gain, and $J$=20 is pumping parameter. The constants $B$=0.012 and $C$=40 describe the transport of charge carriers through carrier–phonon interaction. $\alpha$=2 is the line width enhancement factor, $\gamma_{ns}$=1.0, and $\gamma_{np}$=500. These parameter values are used for the calculated results that are shown in all figures of the paper. The parameters $\Gamma$ and $\tau$ describe the feedback connection and the delay time, respectively. $\Gamma_1$ and $\Gamma_2$ represent the feedback levels governed the mirror reflectivity $R_1$ and $R_2$, respectively. We assume that both facets of the material cavity can be coated to change their reflectivity. The feedback phase $\varphi$ can be tuned by a small current or be controlled with a piezo actuator. Thus, the feedback strengths $\Gamma_1$ and $\Gamma_2$, as well as, the airgap phase $\varphi$ are the main parameters to be varied.

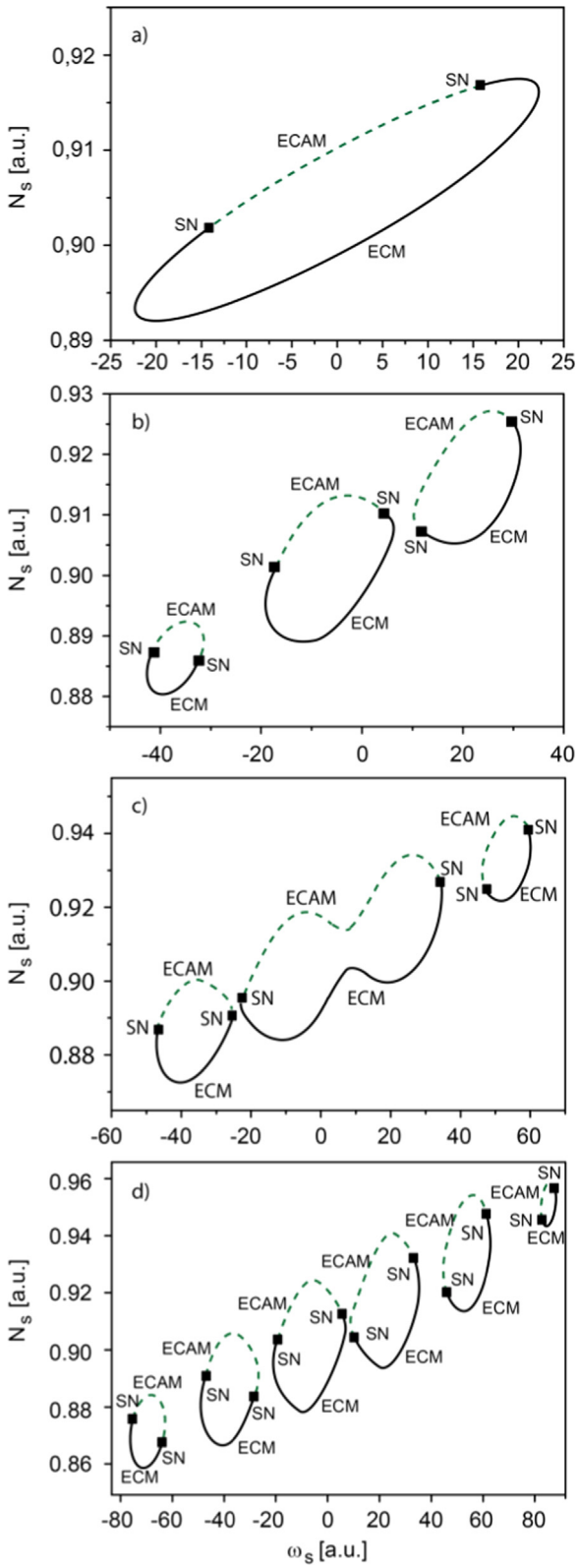


**Fig. 2.** Location of ECMs in the plane of $(N_s-\omega_s)$ for fixed external resonator phase $\psi=\pi/2$, and different feedback strengths (a) $\Gamma_1$=10, $\Gamma_2$=0 (COF), (b) $\Gamma_1$=10, $\Gamma_2$=10, (c) $\Gamma_1$=10, $\Gamma_2$=20, (d) $\Gamma_1$=20, $\Gamma_2$=20. ECAM, external cavity antimodes (dashed green line). SN, saddle-node bifurcation. (For interpretation of the references to color in this figure legend, the reader is referred to the web version of this article.)

## 3. Stationary states

We begin our analysis by considering the stationary lasing

Please cite this article as: S.S. Rusu, et al., Optics Communications (2016), http://dx.doi.org/10.1016/j.optcom.2016.06.082

states of the system (1)–(3). They are given by rotating wave solutions, usually called external cavity modes (ECMs),

$$E = E_s e^{i\omega_s \tau}, \quad N = N_s, \quad \rho = \rho_s. \tag{4}$$

Inserting (4) into (1)–(3) and splitting into real and imaginary parts we obtain a transcendental equation for the emission frequency $\omega_s$

$$\omega_s = -\Gamma_1\left(\alpha\cos(\omega_s\tau_l + \varphi) + \sin(\omega_s\tau_l + \varphi)\right) - \Gamma_2\left[\alpha\cos\left(\omega_s(\tau_l + \tau_L) + \varphi + \psi\right) + \sin\left(\omega_s(\tau_l + \tau_L) + \varphi + \psi\right)\right]. \tag{5}$$

and equations for occupation probability, carrier density and output intensity as follows

$$\rho_s = \frac{1}{2g}\left\{\gamma_{np} + g - 2\left[\Gamma_1\cos(\omega_s\tau_l + \varphi) + \Gamma_2\cos\left(\omega_s(\tau_l + \tau_L) + \varphi + \psi\right)\right]\right\}, \tag{6}$$

$$N_s = -\frac{2B(1-\rho_s)+1}{4C(1-\rho_s)} + \frac{\sqrt{\left[2B(1-\rho_s)+1\right]^2 + 8C(1-\rho_s)J}}{4C(1-\rho_s)}, \tag{7}$$

$$|E_s|^2 = \frac{J - N_s - 2\gamma_{ns}\rho_s}{2(2\rho_s - 1)}. \tag{8}$$

It is well known, that in the case of conventional optical feedback (COF), the case of single cavity the ECMs are located on ellipse. In contrast to the case of COF, the feedback from double cavity resonator implies also a non-elliptic location of modes.

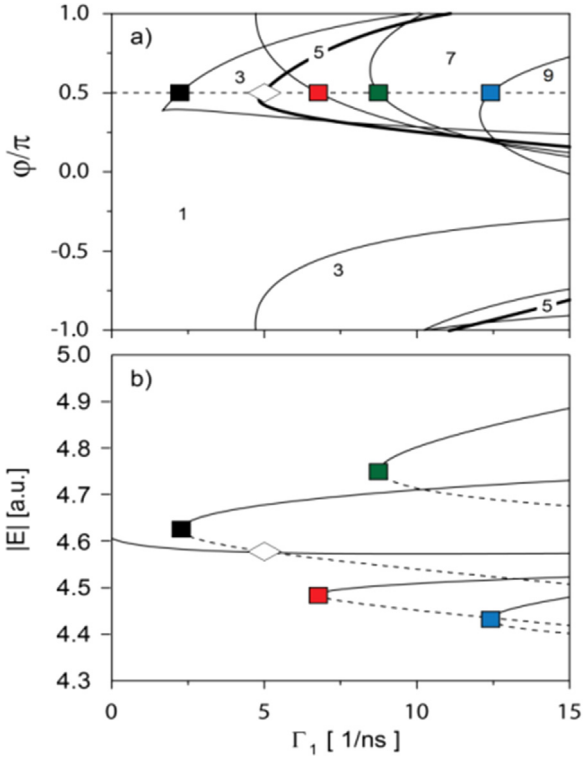


**Fig. 3.** (a) Lines of saddle-node (thin) and transcritical (tick) bifurcations at different locations and number of ECMs in corresponding regions. (b) Bifurcation diagram of the steady states in the plane $|E|$ vs. the feedback strength $\Gamma_1$ for $\varphi=\pi/2$. The solid lines show the modes and dashed lines antimodes. Squares indicate the SN bifurcation. The rhomb denotes transcritical bifurcation. Other parameter: $\Gamma_2=10$.

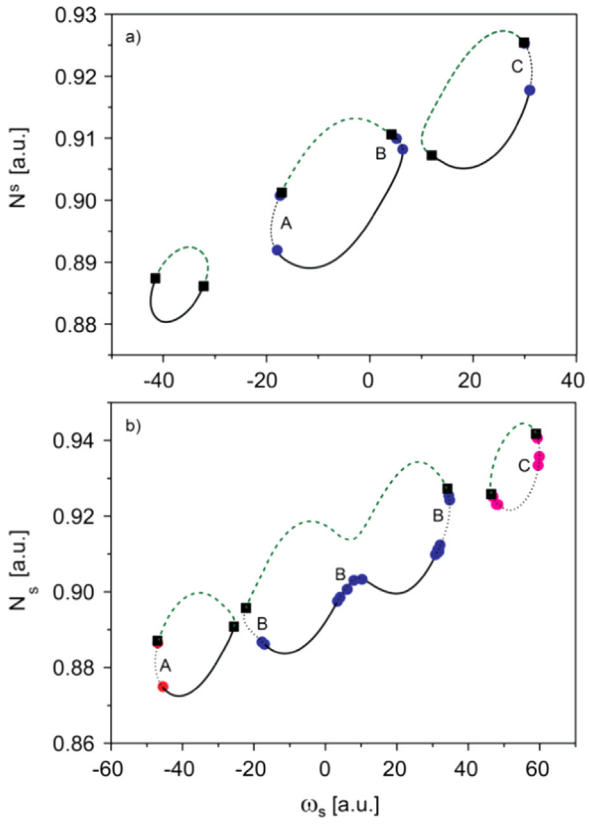


**Fig. 4.** Main bifurcations of system (1)–(3) for $\psi=\pi/2$, and (a) $\Gamma_1=10$, $\Gamma_2=10$, (b) $\Gamma_1=10$, $\Gamma_2=20$, Square, Saddle-Node (SN) bifurcation separating modes (black-stable and red-unstable) and antimodes (green dotted line). Circle, Hopf bifurcation. (For interpretation of the references to color in this figure legend, the reader is referred to the web version of this article.)

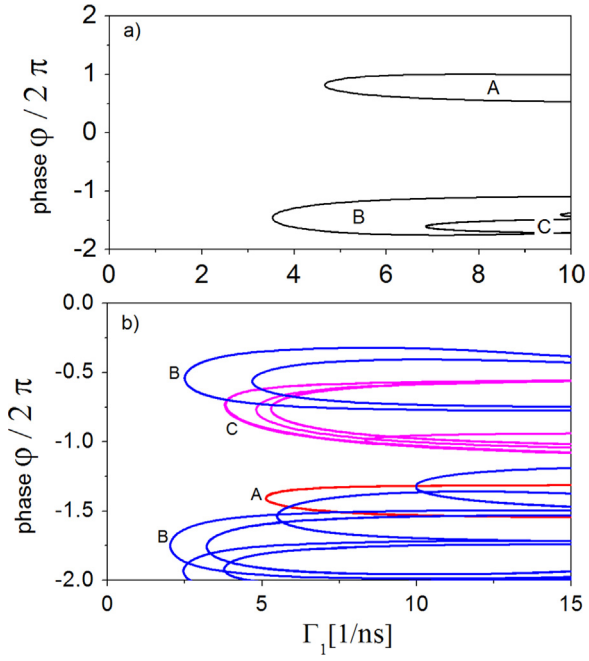


**Fig. 5.** Lines of Hopf bifurcations of stable ECMs for $\psi=\pi/2$ at different locations in the plane $(\varphi-\Gamma_1)$ for (a) $\Gamma_2=10$, and (b) $\Gamma_2=20$.

Fig. 2 shows the locus of ECM in the plane of $(N_s-\omega_s)$ for different vales of feedback strengths.

We first consider the case of $\Gamma_1=10$ and $\Gamma_2=0$ so called conventional optical feedback for which the locations of modes is an

Please cite this article as: S.S. Rusu, et al., Optics Communications (2016), http://dx.doi.org/10.1016/j.optcom.2016.06.082

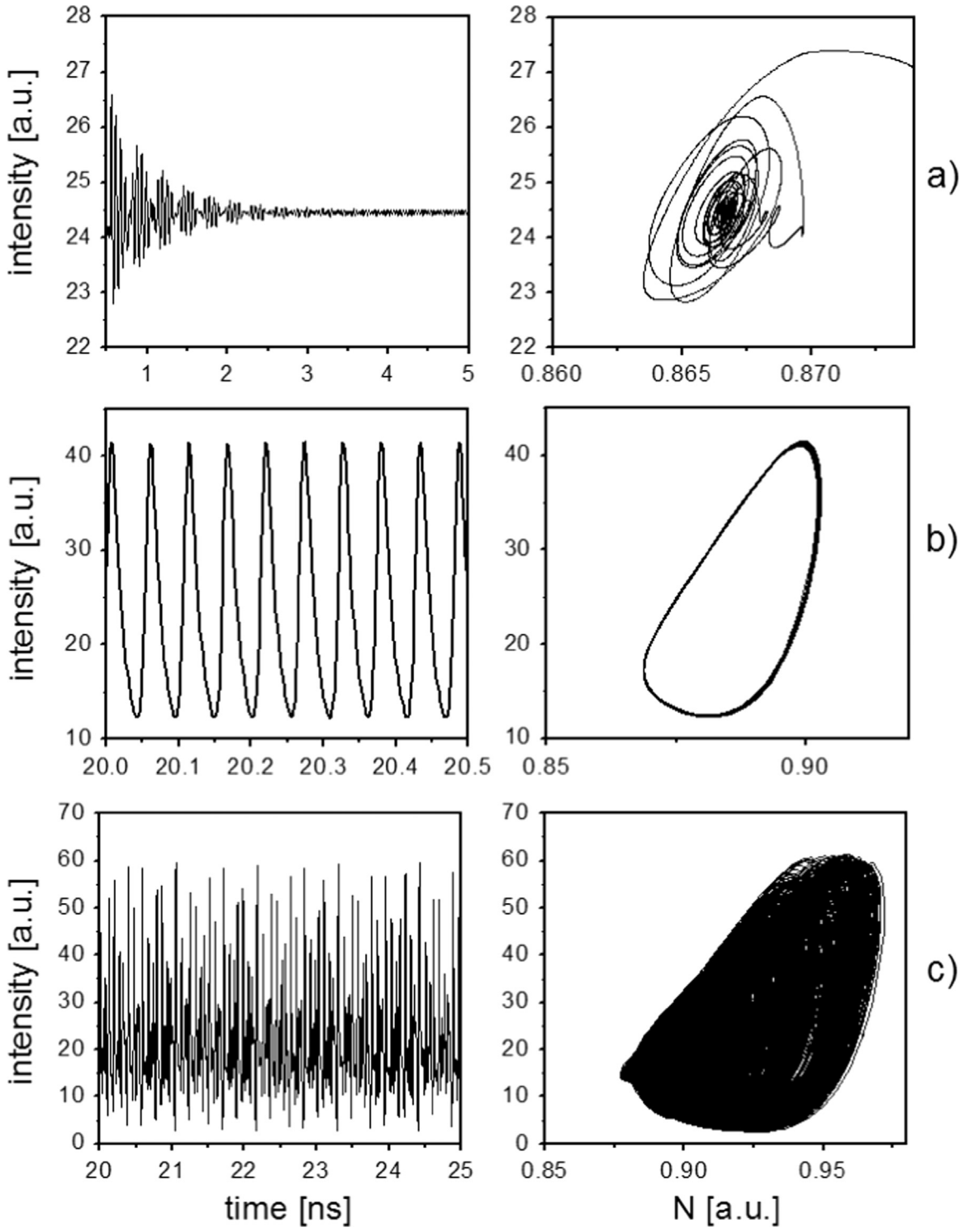


**Fig. 6.** Time evolution of output power (left), and phase portrait in the plane output power P – the density of carrier's $N$ (right) for different values of phase $\varphi$ (a) $\varphi=\pi/2$, CW operation, (b) $\varphi=0$, self-pulsations, and (c) $\varphi=\pi$, chaotic behavior. Other parameters: $\Gamma_1=20$, $\Gamma_2=20$, $\psi=\pi/2$.

ellipse (see Fig. 2(a)). The case of COF was discussed in details since two decades. When the feedback strength $\Gamma_1=10$ and $\Gamma_2$ is increased to 10 the central ellipse is deformed and the outer satellites i.e. bubbles appears (see Fig. 2(b)). As one can see in Fig. 2 (c), when $\Gamma_2$ is increased to 20 the central ellipse is more deformed and is approaching a tilted eight. When both feedback strengths $\Gamma_1$ and $\Gamma_2$ are increased to 20 the ellipse is split into three bubbles of ECMs and additional satellite bubbles appear on the left and right sides (see Fig. 2(d)). It is well known, that the ECMs appear at saddle node bifurcation in pairs so called modes and antimodes. Differentiating (5) we obtain the condition for saddle node bifurcations

$$1 = -\tau_l\Gamma_1\left(-\alpha\ \sin(\omega_s\tau_l+\varphi)+\ \cos(\omega_s\tau_l+\varphi)\right)-(\tau_l+\tau_L)$$
$$\Gamma_2\left[-\alpha\ \sin\left(\omega_s(\tau_l+\tau_L)+\varphi+\psi\right)+\cos\left(\omega_s(\tau_l+\tau_L)+\varphi+\psi\right)\right]. \quad (9)$$

We solved this equation together with (6)–(8) for parameters of Fig. 2. The saddle-node SN points in Fig. 2 separate the ECMs in

Please cite this article as: S.S. Rusu, et al., Optics Communications (2016), http://dx.doi.org/10.1016/j.optcom.2016.06.082

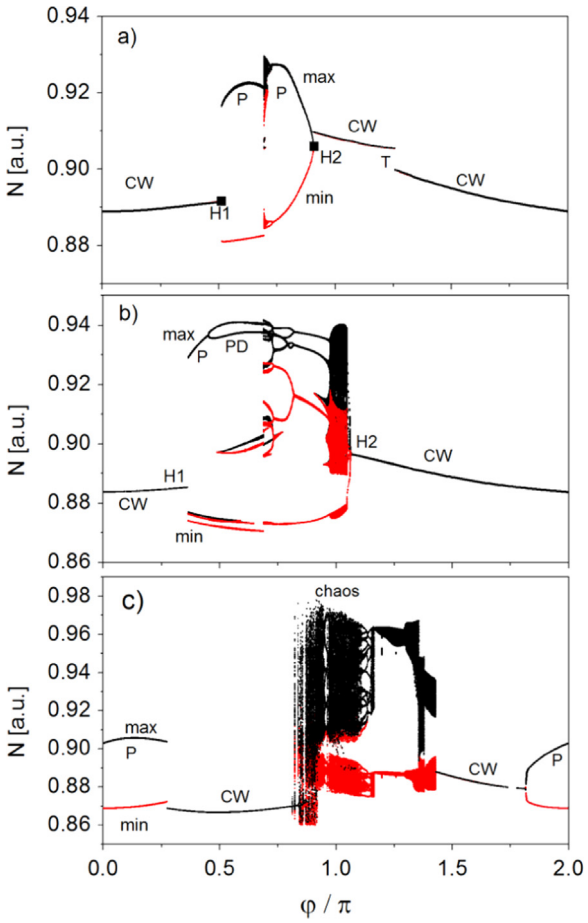


**Fig. 7.** Numerical bifurcation diagram for the phase $\varphi$ being a bifurcation parameter for $\psi=\pi/2$ and different feedback strengths (a) $\Gamma_1=10$, $\Gamma_2=10$, (b) $\Gamma_1=10$, $\Gamma_2=20$, and (c) $\Gamma_1=20$, $\Gamma_2=20$.

saddle and nodes, that are called antimodes and modes. The antimodes are always unstable (dashed line in Fig. 2), while modes may be stable or unstable.

Fig. 3(a) shows the bifurcation scenario when the feedback strength $\Gamma_1$ is the bifurcation parameter. There is a region where only one mode is present. Additional ECMs (in pairs) appear when crossing the SN curve (thin lines). By thick line transcritical bifurcation, obtained from (9), is shown. Fig. 3(b) resembles the situation for fixed $\varphi=\pi/2$ (see dashed line in Fig. 3(a)). Note that each symbol from this line is reproduced in Fig. 3(b).

## 4. Quantum dot laser dynamics

In the following, we use the software DDE-BIFTOOL [24] to investigate the stability of the stationary solutions i.e. of ECMs discussed above, and to find the main bifurcations in the plane of different parameters.

However, we have to mention that for this purpose, it is necessary to use the ECM frequency $\omega_s$ as a reference frequency, which transforms the rotating wave into a stationary solution. In this way, $\omega_s$ is considered as an extra free parameter. To exclude the degeneracy originating from the phase shift invariance, one has to induce an additional constraint, e.g., $\mathrm{Im}E=0$. Fig. 4 show the location of saddle node (square) and Hopf bifurcations (circle) on curves of stationary states for the cases shown in Fig. 2 except that of COF which has been investigated in many references. By solid line we show the stable stationary solutions and by dotted the unstable one. For $\psi=\pi/2$, and $\Gamma_1=\Gamma_2=10$ the all ECMs of left bubble are stable (see Fig. 4(a)).

On the other hand, for middle ellipse and right bubble some modes become unstable (dotted lines) via the Hopf bifurcation (circles). When we increase the feedback strength $\Gamma_2$ to 20 (see Fig. 4(b)) a region of instability appears for ECMs of left bubble. Some ECMs of the middle distorted ellipse are stable (solid line), while others are unstable (dotted lines). For the right bubble, all ECMs are unstable. Thus, an increase of the feedback strength leads to wide unstable regions.

Fig. 5 shows specific Hopf bifurcations in the plane $(\varphi-\Gamma_1)$ for fixed value of phase $\psi=\pi/2$, and different values of $\Gamma_2$. Each unstable region bordered by Hopf bifurcation corresponds to that of Fig. 4. One can see wide regions of instabilities. Thus, in what follows we consider the numerical investigations of solutions of system of (Eqs. (1)–3) to see in more detail of the dynamical behavior.

Fig. 6 shows numerical calculations of pulse traces of the output intensity (left) and phase portrait in the plane of (output intensity–currier density) for different types of dynamical behaviors, where the phase φ is parameter to be changed. Fig. 6(a) shows the continues wave operation, where the stable stationary region contains a stable focus for $\varphi=\pi/2$. Fig. 6(b) presents the time evolution of the output intensity for the regular behavior i.e., self-pulsations, where the phase trajectory becomes a stable limit cycle ($\varphi=0$). The frequency of the pulsation shown in Fig. 6(b) is approximately 20 GHz. When the phase is $\varphi=\pi$, the oscillations of the output intensity become more complicated, the chaotic behavior appears and the phase portrait is a strange attractor (see Fig. 6(c)).

Next we examine the laser dynamics in terms of numerical bifurcation diagrams. The numerically calculated diagrams for different feedback strengths are shown in Fig. 7, where the phase $\varphi$ is the bifurcation parameter and the phase $\psi$ is fixed to $\pi/2$. These figures displays the values of all the local maxima and minima of the time traces of the carrier density. When we increase the phase for $\Gamma_1=10$, $\Gamma_2=10$ the continue wave CW operation is observed (see Fig. 7(a)). Then the laser begins to produce oscillatory behavior through a subcritical Hopf bifurcation H1 in this figure. Since the oscillations are periodic, for a given phase all the local maxima (minima) of the output power have the same value and consequently a single point appears in this figure for the maximum (minimum). The other Hopf bifurcation H2 is supercritical. Only within small region between H1 and H2 we see the non-periodic behavior. A jump between modes can be observed at transcritical bifurcation *T*.

Fig. 7(b) shows the bifurcation diagram for increased feedback strength $\Gamma_2=20$. After periodic solution *P* a period doubling (PD) is observed and a jump to chaotic behavior takes place. For further increase of both feedback strengths $\Gamma_1=20$ and $\Gamma_2=20$ a wide region of strong chaos is present (see Fig. 7(c)). One can see also the torus bifurcation within some region of phase in Fig. 7(c). Finally, we mention that these regions with instabilities and chaos are appropriate for application chaos based communication.

## 5. Conclusions

In this paper we have studied the dynamics of a device composed by a semiconductor laser with active medium quantum dots subject to a double cavity optical feedback. Main advantages of proposed scheme include the existence of two feedback strengths, two feedback phases and two delay times that can be controlled separately. We have treated the setup in the framework of properly adapted Lang-Kobayashi equations. We show that in comparison with conventional optical feedback where the steady states are located on top of an ellipse in the $(N_s-\omega_s)$ plane, in the

Please cite this article as: S.S. Rusu, et al., Optics Communications (2016), http://dx.doi.org/10.1016/j.optcom.2016.06.082

double cavity case the ellipse is distorted and can break into several bubbles. For appropriate feedback strengths that exceed thresholds, an increasing number of additional external cavity modes appear as mode-antimode pairs in saddle node bifurcations. Evaluation, with help of DDE-biftool, of Hopf bifurcations in dependence of magnitude and phase of the feedbacks leads to an understanding of system behavior. In the numerical simulations, the scenario of transition to chaotic behavior from destabilization of relaxation oscillations in Hopf bifurcations to transitions into chaos in dependence of feedback phase was obtained. Thus, bifurcation analysis indicates that various regimes like CW, self-pulsations, period doubling, torus and chaos can occur in a system of semiconductor lasers with active medium quantum dots under se influence of double cavity optical feedback. We believe that our work provides a good basis for future study and, in particular, provides some pointers for more detailed investigations of applications of such devices both for stabilization of laser emission by external cavities and for chaos based communications where appropriate.

## Acknowledgment

Authors acknowledge the support of the projects STCU-5993, 14.02.116 F, and 34/S. VZT acknowledges the support from the Alexander von Humboldt Foundation.

## References

[1] R.F. Kazarinov, Ch.H. Henry, IEEE J. Quantum Electron. 23 (1987) 1401–1409.
[2] R.W.P. Drever, J.L. Hall, F.V. Kowalski, J. Hough, G.M. Ford, A.J. Munley, H. Ward, Appl. Phys. B 31 (1983) 97–105.
[3] B. Dahmani, L. Hollberg, R. Drullinger, Opt. Lett. 12 (1987) 876–878.
[4] C.E. Wieman, L. Hollberg, Rev. Sci. Instrum. 62 (1991) 1–20.
[5] E. Ott, C. Grebogi, J.A. Yorke, Phys. Rev. Lett. 64 (1990) 1196–1199.
[6] V.V. Vassiliev, S.M. Il'ina, V.L. Velichansky, Appl. Phys. B 76 (2003) 521–523.
[7] K. Numata, A. Kemery, J. Camp, Phys. Rev. Lett. 93 (2004) 250602.
[8] E. Schöll, H. G. Schuster (Ed.), Handbook of Cha-os Control, Wiley-VCH, Weinheim, Second completely revised and enlarged edition, 1, 2008, pp. 53–68.
[9] V.Z. Tronciu, H.- J. Wünsche, M. Wolfrum, M. Radziunas, Phys. Rev. E 73 (2006) 046205–046207.
[10] I.V. Ermakov, V.Z. Tronciu, Pere Colet, Claudio R. Mirasso, Opt. Express 17 (2009) 8749–8755.
[11] K. Pyragas, Phys. Lett. 170 (1992) 42–428.
[12] E. Schöll, S.H.L. Klapp, P. Hövel (Eds.), Control of Self-organizing Nonlinear Systems, Springer, Berlin, 2016, pp. 441–460.
[13] E. Schöll, K. Pyragas, Europhys. Lett. 24 (1993) 159–164.
[14] C. Lourenço, A. Babloyantz, Neural Comput. 6 (1994) 1141–1154.
[15] F.R. Ruiz-Oliveras, A.N. Pisarchik, Opt. Express 14 (2006) 12859–12867.
[16] B. Krauskopf, D. Lenstra, Fundamental issues of nonlinear laser dynamics, AIP Conf. Proc. (2000) 548.
[17] A. Argyris, D. Syvridis, L. Larger, V. Annovazzi-Lodi, Pere Colet, Ingo Fischer, Jordi Garcia-Ojalvo, Claudio R. Mirasso, Luis Pesquera, K. Alan Shore, Nature 438 (2005) 343–346.
[18] C.R. Mirasso, G.H.M. van Tartwijk, IEEE J. Quantum Electron. 35 (1999) 764–770.
[19] V. Annovazzi-Lodi, S. Donati, A. Scire, IEEE J. Quantum Electron. 32 (1996) 953–959.
[20] Y. Arakawa, H. Sakaki, Appl. Phys. Lett. 40 (1982) 939–941.
[21] D. Bimberg, M. Grundmann, N.N. Ledentsov, Quantum Dot Heterostructures, British Library, 1999.
[22] G. Huyet, D. O'Brien, S.P. Hegarty, J. Mcinerney, A. Uskov, D. Bimberge, Phys. Status Solidi A 201 (2004) 345–352.
[23] R. Lang, K. Kobayashi, IEEE J. Quantum Electron. 16 (1980) 347–355.
[24] J. Sieber, K. Engelborghs, T. Luzyanina, G. Samaey, D. Roose: DDE-BIFTOOL v.3.1 Manual – Bifurcation analysis of delay differential equations, arxiv.org/abs/1406.7144, August 22, 2015.

Please cite this article as: S.S. Rusu, et al., Optics Communications (2016), http://dx.doi.org/10.1016/j.optcom.2016.06.082